Bulletin of Electrical Engineering and Informatics
Vol. 15, No. 1, February 2026, pp. 209~218
ISSN: 2302-9285, DOI: 10.11591/eei.v15i1.10777

Design and fabrication of a novel millimeter-wave bandstop filter using transversal signal interference technique

Salaheddine Barou[1], Jamal Zbitou[2], Stéphane Ginestar[3], Mohammed El Gibari[3]
[1]Laboratory of Information and Communication Technologies, ENSAT, Abdelmalek Essaâdi University, Tangier, Morocco
[2]National School of Applied Sciences of Tetouan (ENSATe), Abdelmalek Essaâdi University, Tetouan, Morocco
[3]IETR, UMR CNRS 6164, Nantes Université, Nantes, France

Article Info

Article history:

Received May 30, 2025
Revised Oct 5, 2025
Accepted Dec 6, 2025

Keywords:

Bandstop filter
Coplanar waveguide
Microstrip
Millimeter-wave
Transversal signal interference

ABSTRACT

This paper presents the design, simulation, and fabrication of a miniaturized millimeter-wave band-stop filter (BSF) on microstrip technology. The proposed arrangement is based on the concept of transversal interference of signals, and is realized as a pair of parallel transmission lines with the appropriate characteristic impedance and electrical length. Such scheme provides sharpening signal discrimination without resonator structures additional to the filter. The filter is fabricated on a ROGERS RT/Duroid 5880 substrate, selected for its favorable properties at high frequencies, including a thickness of 0.13 mm, a relative dielectric constant of 2.2, and a loss tangent of 0.0009. The optimized design was validated through electromagnetic simulations by two types of electromagnetic solvers, and then fabricated and measured by coplanar waveguide (CPW) probe to confirm its practical performance.

Corresponding Author:

Salaheddine Barou
Laboratory of Information and Communication Technologies, ENSAT, Abdelmalek Essaâdi University
Tangier, Morocco
Email: salaheddine.barou@etu.uae.ac.ma

1. INTRODUCTION

Strict filtering requirements apply to wireless communications in the millimeter wave (mmWave) band, especially in 5G technologies, the internet of things (IoT), and high-speed applications. To guarantee the best radio frequency (RF) performance, compactness, low insertion loss, wide stopband, and signal integrity preservation are crucial. Because they enable interference rejection while still being integrable in small architectures, band-stop filters (BSFs) are essential in this context [1]-[4].

A number of recent methods demonstrate attempts to enhance BSF performance. In order to reconfigure two stopbands with exact geometric control and maintained planarity, Li and colleagues proposed filters that use glide symmetry within substrate-integrated coaxial lines (SICLs) [1], [5], [6]. The structural complexity and lack of adaptability for simultaneous rejection at several frequencies are the approach's drawbacks, though. In order to absorb undesired signals, another line of inquiry investigates so-called quasi-reflectionless filters, which combine coupled lines and resistive elements: an extended stopband was demonstrated by Shao and Lin [3], but the integration of resistors makes this difficult to achieve at high frequencies [7]-[9]. Transverse signal interference (TSI) is the basis for the filters that García and Alonso [10] proposed, and they showed that this principle works well for a variety of filtering functions, including BSF [11]-[14]. In the mmWave band, this method frequently lacks full experimental validation. Additionally, with an isolation of better than 31 dB [3], Moscato and colleagues investigated the direct integration of a

second-order BSF filter into a wideband magnetoelectric dipole antenna for the 24–29.5 GHz and 37–43.5 GHz ranges. This was a convincing solution, but it was less suitable for standalone filter modules.

Although there are still a number of gaps, these works show tremendous progress. Few architectures are able to combine wide stopband, compactness, high selectivity, and straightforward design. For the mmWave band, TSI filters are still not well studied, and experimental validations are frequently not rigorous [10]-[14]. It is frequently challenging to adapt complex structures like glide symmetry or integration into antennas to standard RF modules [1], [5], [6].

In this regard, the current work suggests a novel TSI- BSF filter with a center frequency of 28 GHz that is implemented in microstrip on the ROGERS RT/Duroid 5880 substrate. Excellent agreement between simulations (advanced design system (ADS), momentum, and finite integration technique (FIT) solver) and experimental measurements (PM5 station) is achieved by this architecture, which also achieves a wide fractional stopband (~42.8%) and a high rejection depth. Its simplicity-the lack of intricate resonant structures, ease of fabrication, and compatibility with current RF circuits-defines the approach. This is one of the few mmWave band realizations that we are aware of that combines robust experimental validation, rejection performance, and miniaturization in a TSI architecture [2], [3], [10], [11], [13].

The article's structure is as follows a methodology introduces the filter theory, parameter definition, simulations, manufacturing processes, and measurement protocol; a summary describes the simulated and measured results; a comparison with the state of the art is suggested; tolerances and practical implications are examined; the article concludes with the main contributions, discusses the limitations, and offers ideas for future development toward tunable filters or integration into mmWave RF modules.

2. THEORY AND METHODS

Figure 1 shows the configuration of transversal filtering section with two transmission lines connected in parallel. Each line is characterized by its own impedances (Z_1 and Z_2) as well as electrical lengths (θ_1 and θ_2). This arrangement works by summing the two signal paths in a feedforward manner. While the input signal is divided and sent through each transmission route, the resultant interaction among them creates the desired signal filtering.

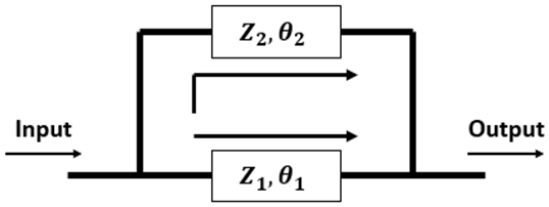

Figure 1. BSF using transversal resonator signal-interference transmission line configuration [10]

Proper tuning of the transversal filtering section comprising the transmission line segments is crucial to maintain the required level of amplitude and phase merging of the signals. One of the main undertakings is to achieve the condition of complete constructive interference at the predefined center frequency. The power transmission and reflection characteristics of this filtering structure, which are referenced to standard impedance Z_0, can be calculated using the admittance parameters of the individual line segments [15].

In order to satisfy the design needs, particular limits must be imposed on the parameters of the transversal section. Foremost among these is the attainment of maximum signal feeding through at the center frequency f_0. Moreover, a balance between the upper and lower sides of the frequency spectrum should be preserved so that a symmetric pass band response about the center frequency f_0 is realized. These design ideas and calculations form the basis of specifying these parameter values to make sure the transversal section achieves the required filtering performance [10].

$$Z_1 > Z_0 \; Z_2 = \frac{Z_1 Z_0}{Z_1 - Z_0} \tag{1}$$

$$\theta_1(f_0) = \frac{m\,\pi}{2}, \; \theta_2(f_0) = (2n + \frac{m}{2})\pi \tag{2}$$

Where $\theta_2 > \theta_1$ is assumed without a loss of generality.

The design parameters were chosen after their effects on the frequency response of the resonator and the viability of physical implementation were examined. The number and location of the transmission zeros,

the stopband bandwidth, and the attenuation level are all determined by the values of θ_1, θ_2, and the impedance ratio $R=Z_2/Z_1$. According to earlier research [16], some combinations, like $\theta_1=\pi$ and $\theta_2=2\pi$ for $R\geq0.5$, offer three transmission zeros but necessitate long lines, which makes compactness more difficult. Others, like $\theta_1=\pi/2$ and $\theta_2=3\pi/2$ for $R\geq1$, produce two zeros with good separation but only optimal attenuation within a small range of R. We chose m=1 and n=1/2 for this work, which led to $\theta_1=90°$ and $\theta_2=270°$ with R=1 ($Z_1=Z_2=100$ Ω). This selection ensures a straightforward and reliable implementation while providing the best possible balance between stopband depth (attenuation greater than 40 dB), bandwidth, and compactness.

The BSF normalized frequency response for various configurations is displayed in Figure 2. The response when the impedance ratio R is set to 1 and when $R\geq1$ is compared in Figure 2(a). It has been found that raising R causes an extra transmission zero to appear, improving the stop band's selectivity while keeping the bandwidth constant. The impact of altering the absolute line impedance for R=1 is shown in Figure 2(b). In this instance, raising the line impedance results in a slight expansion of the rejection bandwidth and an increase in the attenuation depth. A comparison of the two subfigures reveals that the line impedance affects the stop band's width and depth, while the ratio R primarily determines the quantity and location of transmission zeros.

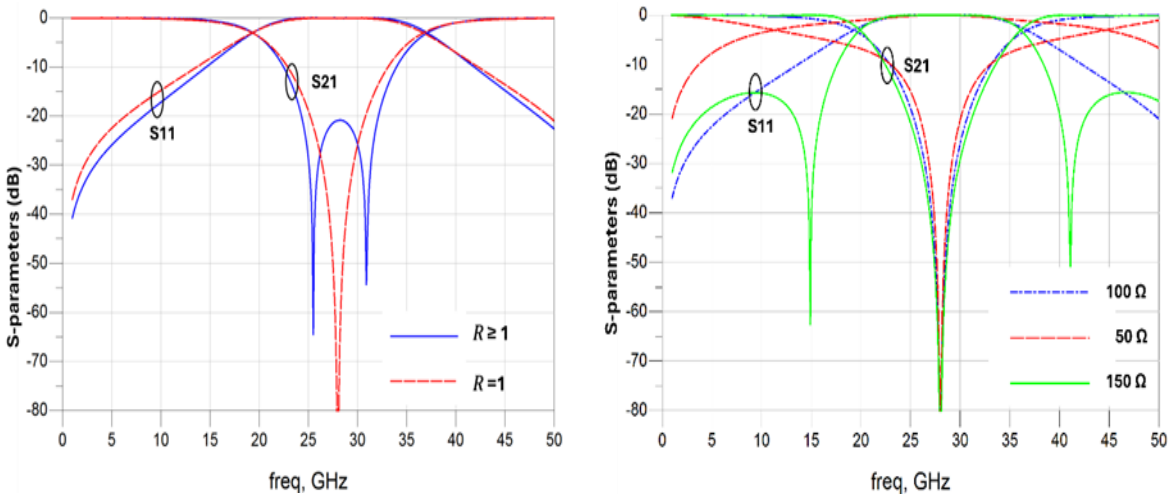

Figure 2. The transversal resonator frequency response ($\theta_1=\pi/2$, $\theta_2=3\pi/2$); (a) comparison for R≥1 and R=1 and (b) comparison for different impedances when R=1

3. RESULTS

In this study presents the validation of a BSF designed with a center frequency of 28 GHz. The configuration of the proposed filter is illustrated in Figure 3. The design exhibits a stopband ranging from 22 GHz to 30 GHz.

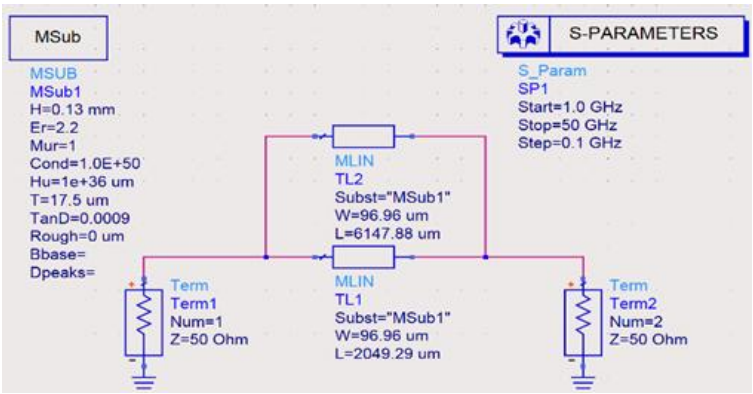

Figure 3. Design of proposed filter simulated by ADS

To assess the accuracy of the theoretical design, simulations were carried out using ADS software. For practical implementation, the filter was fabricated on a ROGERS RT/Duroid 5880 substrate, characterized by a dielectric constant ε_r=2.2, a thickness h=0.13 mm, a loss tangent $tan\ (\delta)$=0.0009, and a metal thickness of t=17.5 µm. This substrate was selected for its excellent electrical stability at high frequencies, exceptionally low dielectric losses, and consistent performance in the millimeter-wave range, making it ideal for achieving the targeted sharp rejection and maintaining minimal signal degradation in compact RF designs.

The frequency response derived from schematic simulation under ADS is shown in Figure 3. The frequency (GHz) is represented by the abscissa axis, while the transmission parameter (dB) is represented by the ordinate axis. The theoretical model is validated by the simulation, which shows a noticeable dip in the stop band around the desired central frequency.

The simulation results in Figure 4 show the proposed bandstop filter works well with high signal suppression and a broad stopband. As already mentioned, the rejection of the signal is high. The transmission coefficient is reported to be as low as -100 dB which further shows substantial attenuation in the rejection band.

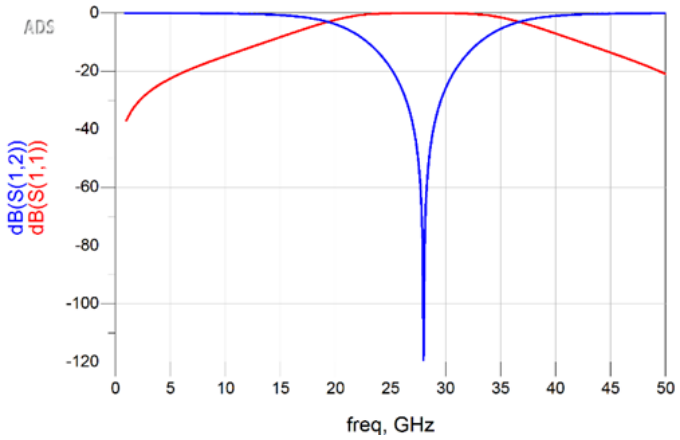

Figure 4. S-parameters versus frequency of the proposed BSF

After the prototype validation of the aforementioned proposed filter, however, it was found that the first transmission line was much broader than the second, which brought an asymmetric layout, and this may have an adverse effect on the electrical performance and compactness of the design. To compensate for this imbalance and reinstate the structural symmetry, the wider line was reconstructed by splitting it into more narrower lines. The alignment of the transmission paths had not only the desired result of sig-nificantly enhancing the physical uniformity of the circuit, but also of allowing a more equal signal distribution per transmission path. The new layout was highly tuned by employing the 'Tuning' feature in the ADS so that the dimensions of the lines could be minutely tuned to maintain the filter performance in desired bands and stopband.

Following the miniaturization step in the ADS schematic environment, the filter structure is displayed in Figure 5. This arrangement demonstrates the geometrical changes made to minimize the circuit footprint while preserving the anticipated stopband and selectivity performance. It is a crucial design step that enables confirmation that the physical dimension reduction is still in line with the theoretical design requirements.

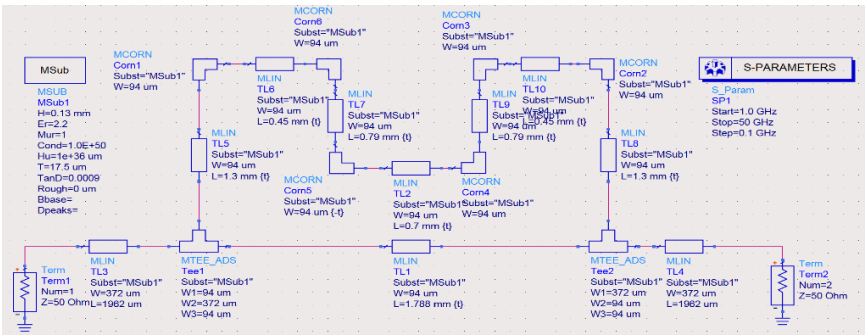

Figure 5. Design of proposed filter simulated by ADS

While maintaining low insertion loss and good matching outside the rejection band, the simulated S-parameters in the Figure 6 display a stopband centered at roughly 28 GHz with strong attenuation (S21<−50dB) and high reflection (S11≈0 dB).

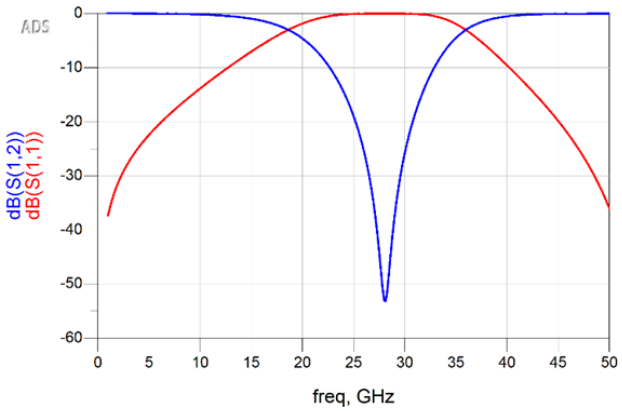

Figure 6. S-parameters versus frequency of ADS

Subsequently, the filter was simulated using the ADS momentum full-wave electromagnetic solver, which enables accurate modeling of distributed effects, coupling, and parasitic phenomena. The results obtained from these simulations were then analyzed to evaluate and validate the filter's performance. Figure 7 illustrates the prototype design using the momentum electromagnetic simulator. The filter displays in Figure 8 a secondary low-frequency rejection near 5–7 GHz in addition to a primary stopband around 28 GHz with deep attenuation (S21<−40 dB) and high reflection (S11≈0 dB). It maintains good matching and low loss outside of these bands.

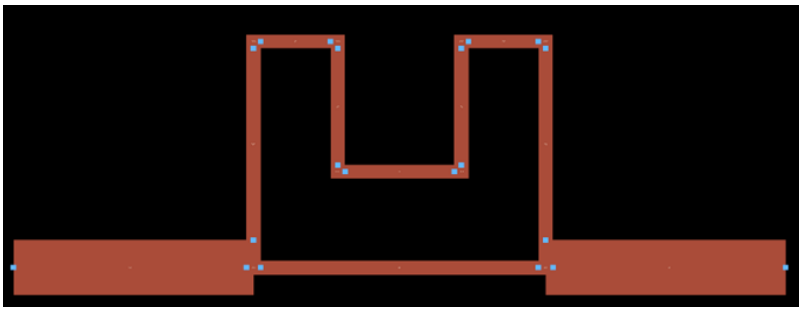

Figure 7. Design of proposed filter simulated by ADS (momentum)

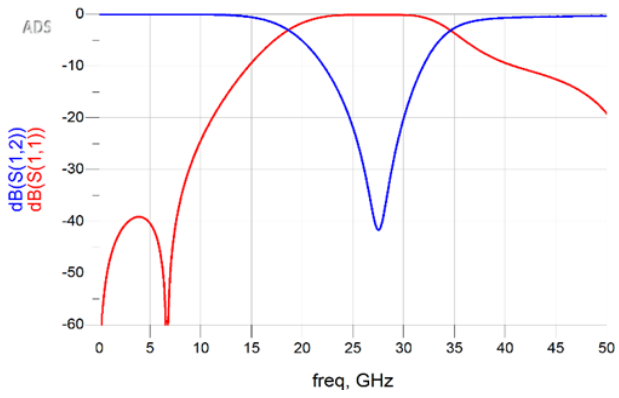

Figure 8. S-parameters versus frequency of ADS (momentum)

The pattern in the response of the filter is clearly observed as a function of the structure simulated in the Figure 9. These differences in the curves can be primarily due to variation in the physical design and boundary conditions used in the simulation. For example, at the level of circuit schematics, parasitic phenomena such as capacitive or inductive crosstalk, or radiation losses can be disregarded, although they can be evaluated with an electromagnetic simulation at higher level. It was observed that the modified structure exhibited performance nearly identical to that of the initial design. To reinforce the reliability of the simulation results obtained in ADS, the analysis was also conducted using an alternative electromagnetic solver based on FIT for cross-validation [17] as shown in Figure 10.

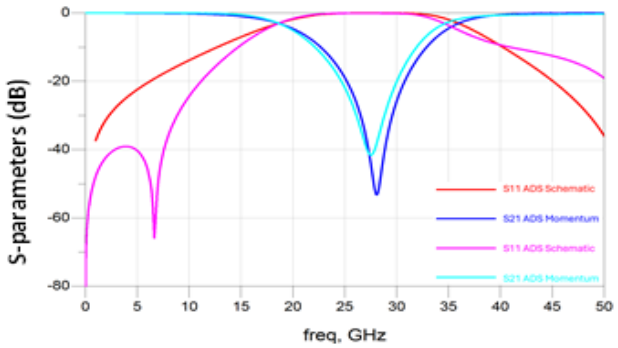

Figure 9. S-parameters versus frequency of ADS (momentum)

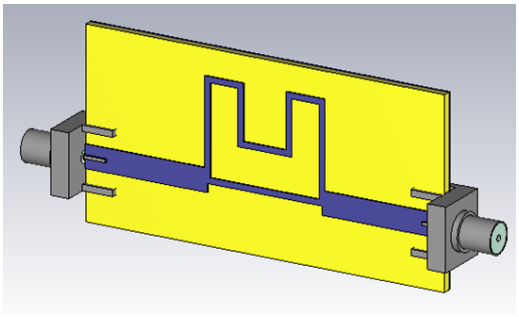

Figure 10. Design of proposed filter simulated by electromagnetic solver

The BSF response in the Figure 11 has a single, distinct attenuation notch at about 28 GHz, where *S*21 falls below -30 dB, signifying a strong rejection of the signal. Good impedance matching outside the stopband is confirmed by the return loss *S*11 staying low close to the notch frequency. This behavior demonstrates how well the filter isolates undesirable frequencies while preserving high transmission in the passbands. The outcomes confirm the anticipated BSF behavior in results with little discrepancies due to the differences in numerical methods used by the electromagnetic solvers.

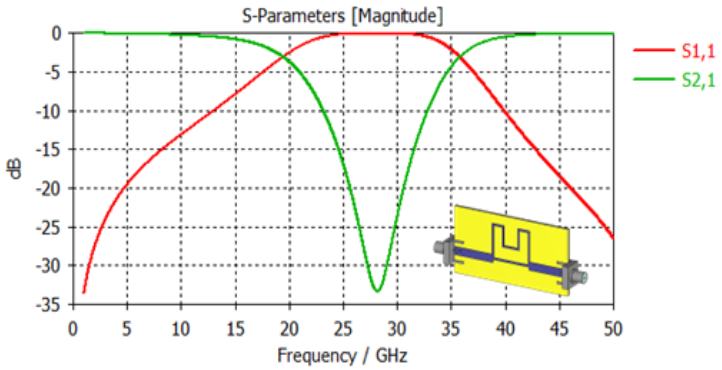

Figure 11. S-parameters versus frequency of electromagnetic solver

4. FABRICATION AND MEASUREMENT

The BSF in Figure 12(a) was fabricated on a ROGERS RT/Duroid 5880 substrate, known for its excellent stability and low dielectric loss at millimeter-wave frequencies. The circuitry was first designed and optimized on ADS and later implemented on the substrate using photolithography and etching methods [18]. Because of the compact and high frequency nature of the design, standard SMA connectors could not provide accuracy for measurement. Instead, the layout was adapted to include CPW probe pads [19], allowing for on-wafer testing using the PM5 probe station shown Figure 12(b) [20], [21]. With this probing technique, accurate and direct signal injection at the test ports as well as evaluation of the filter's performance was made possible. The design accuracy was checked against measured results and simulated data to validate the design accuracy [22].

(a) (b)

Figure 12. Validation step; (a) prototype of the filter manufactured on Rogers RT/Duroid 5880 substrate and (b) PM5 probe station used for millimeter band characterization

Figure 13 presents a comparison between the simulated and measured S-parameters of the proposed bandstop filter. The results show strong agreement across the frequency range, particularly within the stopband centered around 28 GHz. Minor deviations are attributed to fabrication tolerances and measurement conditions, yet the overall consistency confirms the validity of the design.

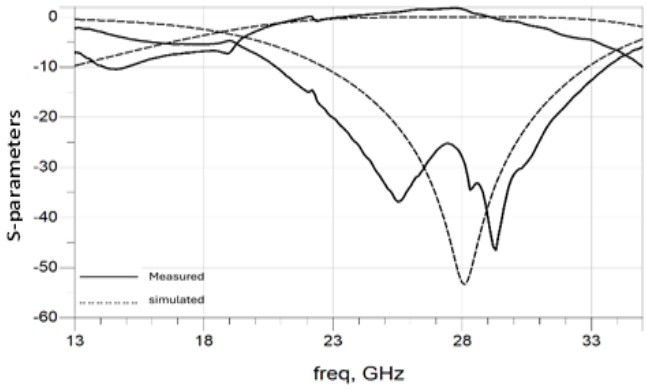

Figure 13. Comparison between simulated and measured results

Figure 13 shows the remaining differences between measurements of the filter and its simulation. It may be very well that these differences are due in the first place to the practical limitations of the measurements. An important contributor is most likely the accuracy of the probe positioning system. If the probe can be attached to the circuit in a non-moving fashion, the perfect connection at richer millimeter-wave frequencies brings another set of problems. Some level of variation also results from the attachment of CPW probe-fed ports rather than standard connectors, the impedance environments of which have their own influence on the system. Together they all go some way to explain the discrep-ancy with the theoretical efficiency. A comparison is made between the performance of the current BSF and the previously published BSF, and the results are summarized in Table 1.

Table 1. Performance comparison with recently published

References	Center frequency (GHz)	Fractional bandwidth (%)	Insertion loss (dB)	Technology	Filter size (mm²)
[23]	60	21	-	0.18 µm CMOS	0.52×0.77
[24]	60	16.66	18	0.18 µm CMOS	-
[25]	32	10	-	GaAs	2.5×2
[15]	60	91.6	4	0.18 µm CMOS	0.78×0.77
	55	90.9	2.5		1.51×0.32
This work	28	42.85	5.52	MICROSTRIP	5.9×3

With a fractional bandwidth of 42.85%, the suggested 28 GHz filter is noticeably more expansive than earlier designs. Although it has a higher insertion loss (5.52 dB) than some CMOS or GaAs designs, it is still manageable given the bandwidth attained and the microstrip technology. The ease of integration on RF substrate and ease of manufacturing make up for the larger dimensions (5.9×3 mm²) compared to integrated circuits. Loss reduction, miniaturization through defected ground structure (DGS) or multilayer structures, and expansion to multi-band versions could all be improvements.

5. CONCLUSION

This work has revealed the reliability of design, simulation, and fabrication on a compact millimeter–wave bandstop filter based on the transversal signal interference principle. The filter has been optimised for sharp rejection at around 28 GHz by es-tablishing precise modelling in ADS and electromagnetic solver with FIT. The fabricated prototype on ROGERS RT/Duroid 5880 substrate vali-dates the proposed method in terms of electrical performance and physical integration. Manufacturing tolerances, limitations on coplanar probe measurement, and the fixed stop band's nature, which restricts the device's reconfigurability, are the primary causes of the observed deviations. Opportunities for improvement include creating tunable versions, integrating them into small RF modules, and optimizing them for different frequency ranges. Targeted interference suppression is essential for enhancing signal quality and guaranteeing effective spectral coexistence in millimeter-wave 5G and IoT systems, where this kind of design holds great promise.

This work can be expanded upon in a number of ways in future studies. Multi-band operation and dynamic frequency adaptation may be made possible by the incorporation of tunable or reconfigurable components into SRR. Manufacturability would be improved by further optimizing the layout to increase tolerance robustness and decrease sensitivity to fabrication errors. Furthermore, the suggested filter may offer small and versatile solutions for new wireless technologies when combined with antenna systems or front-end modules.

ACKNOWLEDGMENTS

The authors thank the managers of the IETR platforms: MATRIX for fabrication and M2ARS for on-wafer characterization.

FUNDING INFORMATION

Authors state no funding involved.

AUTHOR CONTRIBUTIONS STATEMENT

This journal uses the Contributor Roles Taxonomy (CRediT) to recognize individual author contributions, reduce authorship disputes, and facilitate collaboration.

Name of Author	C	M	So	Va	Fo	I	R	D	O	E	Vi	Su	P	Fu
Salaheddine Barou	✓	✓	✓	✓	✓	✓		✓	✓	✓			✓	
Jamal Zbitou	✓	✓		✓	✓	✓	✓	✓	✓	✓	✓	✓	✓	
Stéphane Ginestar	✓	✓			✓	✓	✓	✓	✓	✓	✓	✓		
Mohammed El Gibari	✓	✓			✓	✓	✓	✓	✓	✓	✓	✓		

C : **C**onceptualization
M : **M**ethodology
So : **So**ftware
Va : **Va**lidation
Fo : **Fo**rmal analysis
I : **I**nvestigation
R : **R**esources
D : **D**ata Curation
O : Writing - **O**riginal Draft
E : Writing - Review & **E**diting
Vi : **Vi**sualization
Su : **Su**pervision
P : **P**roject administration
Fu : **Fu**nding acquisition

CONFLICT OF INTEREST STATEMENT

Authors state no conflict of interest.

DATA AVAILABILITY

Data availability is not applicable to this paper as no new data were created or analyzed in this study.

REFERENCES

[1] X. Li *et al.*, "Band-Stop Filter Based on Glide-Symmetric Substrate-Integrated Coaxial Lines for Band-Gap Control and Bandwidth Customization," *Physical Review Applied*, vol. 19, no. 2, p. 024018, Feb. 2023, doi: 10.1103/PhysRevApplied.19.024018.

[2] V. N. R. Vanukuru and V. K. Velidi, "Millimeter-Wave CMOS 30/80 GHz Sharp-Rejection Dual-Band Bandstop Filters Using TFMS Open-Stepped-Impedance Resonators," *IEEE Transactions on Circuits and Systems II: Express Briefs*, vol. 68, no. 1, pp. 201–205, 2021, doi: 10.1109/TCSII.2020.3006198.

[3] J. Y. Shao and Y. S. Lin, "Millimeter-wave bandstop filter with absorptive stopband," *IEEE MTT-S International Microwave Symposium Digest*, Tampa, FL, USA, Jun 2014, doi: 10.1109/MWSYM.2014.6848584.

[4] K. Salehian and M. Tayarani, "A novel SIGGW dual post band-pass filter for 5G millimeter-wave band applications with a transmission zero," *Scientific Reports*, vol. 13, no. 1, p. 20743, Nov. 2023, doi: 10.1038/s41598-023-47490-1.

[5] A. T. Dominguez, J. M. F. González, and O. Q. Teruel, "Mechanically Reconfigurable Waveguide Filter Based on Glide Symmetry at Millimetre-Wave Bands," *Sensors*, vol. 22, no. 3, 2022, doi: 10.3390/s22031001.

[6] M. Karamirad *et al.*, "Low-loss and dual-band filter inspired by glide symmetry principle over millimeter-wave spectrum for 5G cellular networks," *iScience*, vol. 26, no. 1, p. 105899, Jan. 2023, doi: 10.1016/j.isci.2022.105899.

[7] S. Moscato, S. Caicedo, and M. Oldoni, "Bandpass filter with multiple selective absorptive stopbands for 28 GHz transmitters," *International Journal of Microwave and Wireless Technologies*, 2024, doi: 10.1017/S1759078724000394.

[8] Y.-H. Zhu, X.-Y. Fang, X. Xie, L.-L. Yang, and J.-X. Chen, "Two-Port Reflectionless Waveguide Bandpass Filter for Indoor Distribution Systems," *SSRN*, 2023, doi: 10.2139/ssrn.4635309.

[9] M. R. A. Nasser and D. Psychogiou, "Reflective and quasi-reflectionless multiband bandpass filters using multi-resonant acoustic-wave lumped-element resonators," *International Journal of Microwave and Wireless Technologies*, vol. 17, no. 2, pp. 318–330, 2025, doi: 10.1017/S1759078724001211.

[10] R. G. García and J. I. Alonso, "Design of sharp-rejection and low-loss wide-band planar filters using signal-interference techniques," *IEEE Microwave and Wireless Components Letters*, vol. 15, no. 8, pp. 530–532, 2005, doi: 10.1109/LMWC.2005.852797.

[11] R. G. García, L. Yang, and J. M. M. Ferreras, "Optimisation-based design of transversal signal-interference microwave bandpass and lowpass filters with extended stopband," *IET Microwaves, Antennas and Propagation*, vol. 15, no. 6, pp. 653–660, 2021, doi: 10.1049/mia2.12091.

[12] H. Y. Zhang *et al.*, "Compact transversal signal-interaction wideband bandpass filter with multiple transmission zeros and wide stopband," *AEU - International Journal of Electronics and Communications*, vol. 185, 2024, doi: 10.1016/j.aeue.2024.155449.

[13] L. Wang *et al.*, "Design of high selectivity tri-band bandpass filter based on triple transversal transmission path," *AEU - International Journal of Electronics and Communications*, vol. 181, p. 155347, Jul. 2024, doi: 10.1016/j.aeue.2024.155347.

[14] L. Yang, M. Malki, X. Zhu, and R. G. García, "Multilayer signal-interference fourth-order high-selectivity dual-band bandpass filter with multiple transmission zeros," *International Journal of Microwave and Wireless Technologies*, vol. 17, no. 4, pp. 595–602, May 2025, doi: 10.1017/S1759078725000492.

[15] M.-L. Her, Q.-M. Lin, K.-Y. Lin, Y.-D. Wu, and Y.-L. Wang, "Dual-mode and three-transmission-zeros bandstop filters with closed-loop ring resonators," *Microwave and Optical Technology Letters*, vol. 44, no. 2, pp. 114–118, Jan. 2005, doi: 10.1002/mop.20562.

[16] M. K. Mandal and P. Mondal, "Design of sharp-rejection, compact, wideband bandstop filters," *IET Microwaves, Antennas and Propagation*, vol. 2, no. 4, pp. 389–393, 2008, doi: 10.1049/iet-map:20070212.

[17] L. Codecasa and L. Di Rienzo, "Stochastic Finite Integration Technique for Eddy-Current Problems," in *IEEE Transactions on Magnetics*, vol. 51, no. 3, pp. 1-4, Mar. 2015, doi: 10.1109/TMAG.2014.2356716.

[18] J. Hong and M. J. Lancaster, "Microstrip Filters for RF/Microwave Applications," *Microstrip Filters for RF/Microwave Applications*, New York, NY, USA: Wiley, 2001.

[19] G. N. Phung and U. Arz, "Modeling and Analytical Description of Parasitic Probe Effects in Measurements of Conductor-Backed Coplanar Waveguides," *Advances in Radio Science*, vol. 20, pp. 119–129, 2023, doi: 10.5194/ars-20-119-2023.

[20] K. Zhao *et al.*, "Time Domain Simulated Characterization of the Coplanar Waveguide in an On-Chip System for Millimeter Waveform Metrology," *Electronics (Switzerland)*, vol. 13, no. 1, 2024, doi: 10.3390/electronics13010145.

[21] J. Zhu, Z. Wan, and K. Zhao, "Method to Change the Through-Hole Structure to Broaden Grounded Coplanar Waveguide Bandwidth," *Sensors*, vol. 23, no. 9, p. 4342, 2023, doi: 10.3390/s23094342.

[22] D. M. Pozar, "Microwave Engineering," 4th ed. Hoboken, NJ, USA: Wiley, 2011.

[23] V. N. R. Vanukuru, V. K. Velidi, and A. Chakravorty, "60 GHz millimeter-wave compact TFMS bandstop filter using transversal resonator in 0.18µm CMOS technology," *IEEE MTT-S International Microwave and RF Conference 2014, IMaRC 2014 - Collocated with International Symposium on Microwaves (ISM) 2014*, 2014, pp. 248–250, doi: 10.1109/IMaRC.2014.7039019.

[24] X. Y. Li and M. S. Tong, "A Bandstop Filter Based on Inverted Microstrip Gap Waveguide for Millimeter-Wave Communications," *2022 IEEE International Symposium on Antennas and Propagation and USNC-URSI Radio Science Meeting, AP-S/URSI 2022 - Proceedings*, pp. 549–550, 2022, doi: 10.1109/AP-S/USNC-URSI47032.2022.9886555.

[25] K. Y. E. Chan and R. Ramer, "Millimeter-wave reconfigurable bandpass filters," *International Journal of Microwave and Wireless Technologies*, vol. 7, no. 6, pp. 671–678, 2015, doi: 10.1017/S1759078714001214.

BIOGRAPHIES OF AUTHORS

Salaheddine Barou was born in 1998 in Casablanca, Morocco, currently pursuing a Ph.D. at the National School of Applied Sciences (ENSA) Tangier within Abdelmalek Essaadi University. Having obtained a master's degree in automatic signal processing and industrial computing in 2020, his ongoing research is centered on the design of new planar filtering structures for millimeter-band applications. He can be contacted at email: salaheddine.barou@etu.uae.ac.ma.

Pr. Dr. Jamal Zbitou was born in Fes, Morocco, in June 1976. He received the Ph.D. degree in electronics from Polytech of Nantes, the University of Nantes, France, in 2005. He is currently Full Professor of Electronics in ENSA of Tetuan, Abdelmalek Essaadi University Morocco. He is involved in the design of hybrid, monolithic active and passive microwave electronic circuits. He is involved also in the design of rectennas, RFID tag and their applications in wireless communications, and wireless power transmission (WPT). He is the General Chair of the International Conference on Computing and Wireless Communication Systems (www.iccwcs.net). He is the author/co-author of more than 205 scientific Scopus Indexed publications and Editor of Four Handbooks and Book, and thesis advisor and Co-advisor of 35 Ph.D. students. He can be contacted at email: j.zbitou@uae.ac.ma.

Stéphane Ginestar obtained his Ph.D. in 2009 from the Institut d'Électronique, de Microélectronique et de Nanotechnologie (IEMN). He is currently the head of the cleanroom facility in Nantes and co-head of the MATRIX platform at IETR. His main mission is to provide the institute with technological support for the development and integration of multifunctional thin-film materials—featuring tunable permittivity, piezoelectric, electromechanical, and electro-optical properties—into components and sub-components for innovative telecommunications applications, within the framework of the laboratory's research projects. He can be contacted at email: stephane.ginestar@univ-nantes.fr.

Mohammed El Gibari is an Associate Professor at Nantes University, received his Ph.D. and HdR from Nantes University respectively in 2009 and 2025. His current research activities at the Institut d'Électronique et des Technologies du NuméRique (IETR) focus on three main areas: The first concerns the development of opto-microwave components based on thin-film polymers, with particular emphasis on microwave access for modulators and analog-to-digital converters. The second area investigates the impact of nanoparticle integration on the electro-optical properties of polymer materials. Finally, his work includes the design and fabrication of piezoelectric sensors, as well as implantable piezoresistive blood pressure sensors for medical applications. He is author and co-author of over 80 articles and conferences. He can be contacted at email: mohammed.el-gibari@univ-nantes.fr.